

Bulk Enthalpy of Melting of Poly (L-lactic acid) (PLLA) Determined by Fast Scanning Chip Calorimetry

Katalee Jariyavidyanont, Mengxue Du, Qiang Yu, Thomas Thurn-Albrecht, Christoph Schick, and René Androsch*

The bulk enthalpy of melting of α -crystals of poly (L-lactic acid) (PLLA) is evaluated by fast scanning calorimetry (FSC), by correlating the melting enthalpy of samples of different crystallinity with the corresponding heat capacity at 90 °C, that is at a temperature higher than the glass transition temperature of the bulk amorphous phase and lower than the melting temperature. Extrapolation of this relationship for crystals formed at 140 °C towards the heat capacity of fully solid PLLA yields a value of $104.5 \pm 6 \text{ J g}^{-1}$ when melting occurs at 180–200 °C. The analysis relies on a two-phase structure, that is, absence of a vitrified rigid amorphous fraction (RAF) at the temperature of analysis the solid fraction (90 °C). Formation and vitrification of an RAF are suppressed by avoiding continuation of primary crystallization and secondary crystallization during cooling the system from the crystallization temperature of 140 °C to 90 °C, making use of the high cooling capacity of FSC. Small-angle X-ray scattering (SAXS) confirmed thickening of initially grown lamellae which only is possible if these lamellae are not surrounded by a glassy RAF. Linear crystallinity values obtained by SAXS and calorimetrically determined enthalpy-based crystallinities agree close to each other.

1. Introduction

The properties and therefore fields of application of crystallizable polymers depend to a large degree on the presence of crystals.^[1–3] For this reason, knowledge of the fraction of crystals, commonly abbreviated “Crystallinity,” is of superior importance to assure property profiles and to establish processing–structure–property relations. The crystallinity of polymers can be assessed by many characterization techniques, including X-ray scattering, density measurements, or calorimetry, with each method having specific advantages and shortcomings.^[4–7] Differential scanning calorimetry (DSC) may be considered as one of the most often used tools to obtain crystallinity-data, related to its wide availability, rather easy use, and relatively—at least at first sight—simple data evaluation.^[7] For evaluation of the crystallinity, in a typical DSC-experiment, the sample of interest is heated to allow

melting of crystals. The area of the melting peak, observed at the melting temperature T_m , yields the enthalpy of melting $[\Delta h_m(T_m)]$ and provides first information about the possible presence of crystals. After normalization with the bulk enthalpy of melting $[\Delta h_{m,100}(T_m)]$, that is, the specific enthalpy of melting of a volume-element inside the crystal, being equivalent to the specific enthalpy of melting of a 100%-crystalline sample at the temperature of the observed melting peak, the so-called enthalpy-based crystallinity $X_{c,DSC} [= \Delta h_m(T_m) / \Delta h_{m,100}(T_m)]$ is observed.^[4–7] While the experimental observation of $\Delta h_m(T_m)$ for an experienced instrument operator, based on the use of a calibrated instrument and state-of-the-art corrections of the measured DSC curve,^[8] is considered laboratory routine, its recalculation into a crystallinity-value relies on the selection of a valid value of $\Delta h_{m,100}(T_m)$. Note, this value holds only for crystals that melt at T_m and is different from the bulk enthalpy of melting at the equilibrium melting temperature $T_{m,0}$ $[\Delta h_{m,100}(T_{m,0})]$. Unfortunately, for poly(L-lactic acid) (PLLA), as one of the most important biobased polymers,^[9] unequivocal information $\Delta h_{m,100}$ -values of α' - and α -crystals which develop on melt-crystallization below and above 110–120 °C, respectively, does not exist, leading to great uncertainty in the determination of the enthalpy-based crystallinity. In short, $\Delta h_{m,100}$ -values for α -crystals scatter between around 90 and 200 J g^{-1} while for the disordered

K. Jariyavidyanont, M. Du, R. Androsch
Interdisciplinary Center for Transfer-oriented Research in Natural Sciences

Martin Luther University Halle-Wittenberg
06099 Halle/Saale, Germany
E-mail: rene.androsch@iw.uni-halle.de

Q. Yu, T. Thurn-Albrecht
Institute of Physics
Martin Luther University Halle-Wittenberg
06099 Halle/Saale, Germany

C. Schick
University of Rostock
Institute of Physics and Competence Center CALOR
Albert-Einstein-Str. 23–24, 18059 Rostock, Germany

C. Schick
Butlerov Institute of Chemistry
Kazan Federal University
18 Kremlyovskaya Street, Kazan 420008, Russia

 The ORCID identification number(s) for the author(s) of this article can be found under <https://doi.org/10.1002/marc.202200148>

© 2022 The Authors. Macromolecular Rapid Communications published by Wiley-VCH GmbH. This is an open access article under the terms of the Creative Commons Attribution License, which permits use, distribution and reproduction in any medium, provided the original work is properly cited.

DOI: 10.1002/marc.202200148

α' -crystal polymorph values between 57 and 107 J g⁻¹ are reported.^[10–21]

In order to contribute to the further evaluation of the bulk enthalpy of melting of α -crystals of PLLA, in this work fast scanning chip calorimetry (FSC) was employed, for analysis of the correlation between the measured enthalpy of melting of a set of samples of different crystallinity on one side and the corresponding change of the heat capacity at a temperature higher than the glass transition temperature (T_g) of ≈ 60 °C^[22,23] and lower than the onset temperature of the melting process on the other side. Since the heat capacity of a polymer at temperatures higher than T_g depends on the solid fraction,^[24] extrapolation of this relationship toward the heat capacity of solid PLLA yields the bulk enthalpy of melting. A similar approach, using the heat-capacity step at T_g instead the heat capacity at a slightly higher temperature, has been applied in the past.^[15,20,21] It relies on the assumption of a two-phase structure, that is, the presence of a liquid amorphous phase and of solid crystals between T_g and the final melting temperature only. However, the presence of a two-phase structure in semicrystalline PLLA is debated and formation of a rigid amorphous fraction (RAF)^[25,26] related to the crystallization process is frequently suggested.^[27–30] For crystallization at 145 °C, there is proposed that at the crystallization temperature no vitrification of the amorphous phase, or parts of it, occurs but on subsequent slow cooling, to yield a glassy amorphous fraction of close to 0.2 at 120 °C, continuously increasing on further lowering the temperature.^[30]

In a recent study,^[31] similar as in case of poly(butylene succinate) (PBS),^[32] we suggested that annealing of PLLA at temperatures lower than the temperature of primary crystallization of 140 °C causes secondary crystallization and formation of small crystals of lower melting temperature than in case of the lamellae formed during primary crystallization. The time dependence of the formation of secondary crystals on isothermal low-temperature-annealing of PLLA crystallized at higher temperature predicts that it also occurs as a continuous process during cooling at rates typically applied in a DSC, thus contributing to measured heat-flow rates and complicating analyses of the phase structure. Fast cooling, however, can outpace secondary crystallization, allowing to obtain unequivocal information about the heat capacity describing the solid fraction of the system. As a working hypothesis, with the use of FSC, at least suppression of RAF-formation and -vitrification during cooling, caused by secondary insertion crystallization, is assumed, allowing then analysis of the bulk enthalpy of melting of α -crystals of PLLA via correlating the enthalpy of melting with the heat capacity slightly above T_g , based on the validity of a two-phase structure. A further advantage of using FSC is the suppression of crystal reorganization and melt-recrystallization during heating, which simplifies the evaluation of enthalpies of melting.^[33,34]

The presentation of results below is structured such that in the first part the correlation between the heat capacity slightly above T_g and the enthalpy of melting, both based on isothermal crystallization experiments at 140 °C, is explained. This is followed by providing small-angle X-ray scattering (SAXS) data collected on samples subjected to secondary crystallization at 140 °C for different time, yielding linear crystallinities and conclusions about lamellar thickening. Finally, in the third part, FSC experiments to prove the absence of crystallization and RAF for-

mation/vitrification on cooling and the validity of a two-phase structure are presented.

2. Experimental Section

2.1. Materials

An extrusion-grade PLLA homopolymer, grade L175 from Corbion (Netherlands), with a D-isomer content of <1%, a mass-average molar mass of 120 kg mol⁻¹, and melt-flow rate of 8 g/(10 min) (210 °C/2.16 kg) was used.^[35,36] The material was delivered in the form of pellets and prepared for the various FSC, DSC, and SAXS experiments as described below. For re-evaluation of the magnitude of the heat-capacity step of fully amorphous samples at the glass transition, needed for estimation of the mass of FSC samples, besides the above described PLLA-homopolymer, also a non-crystallizable racemic PDLLA copolymer (Resomer R 207 S, Evonik, Germany) with a mass-average molar mass and polydispersity of 262 kg mol⁻¹ and 1.6, respectively, and containing 50% L- and D-co-units, was employed.^[37] Using noncrystallizable PDLLA for determination of the heat-capacity increment at T_g is considered advantageous compared to crystallizable PLLA, as on heating cold-crystallization is absent, allowing therefore a safer construction of tangents for obtaining the heat-capacity step at T_g .

2.2. Instrumentation

Fast Scanning Chip Calorimetry (FSC): A Flash DSC 1 (Mettler-Toledo, Greifensee, Switzerland) was used. The instrument was operated in conjunction with a TC 100 intracooler (Huber, Offenbach, Germany), allowing to set the sample-support temperature to -90 °C. The sensor/sample compartment was purged with nitrogen at a flow rate of 40 mL min⁻¹. Samples were prepared by cutting sections of 8 μ m thickness using a rotary microtome (Slee, Mainz, Germany). These sections were afterward reduced in their lateral size to 50–100 μ m, using a stereomicroscope and a scalpel. Such samples had a mass of ≈ 100 ng, assuring negligible thermal lag, as analyzed by the heating rate-dependence of T_g ,^[38,39] and sufficient signal-to-noise ratio on cooling and heating at a rate of 1000 K s⁻¹. Before loading the sample onto the UFS 1 chip sensor, the latter was conditioned and temperature-corrected according to the instrument specifications. Afterward, first a thin layer of silicone oil was spread on the sensor, followed by placing a layer of gold-leaf in the center of the heatable area where a homogeneous temperature-distribution is evident.^[40,41] Such setup assures optimum thermal contact between sample and sensor and also reduces mechanical distortion of the sensor membrane during heating and cooling, related to the different thermal expansion coefficients of the polymer sample and silicon nitride membrane, as well as during crystallization and melting of the polymer. Such distortion of the membrane causes a change in the instrumental baseline and complicates, e.g., analysis of heat capacities.

Differential Scanning Calorimetry: Complementary calorimetric analysis of the heat-capacity step at T_g , for the sake of estimating the mass of FSC samples, was performed using a calibrated

heat-flux DSC 1 (Mettler-Toledo, Greifensee, Switzerland), operated in conjunction with a TC 100 intracooler. The furnace was purged with nitrogen at a flow rate of 60 mL min^{-1} . Regarding the analysis of the heat-capacity step at T_g , samples with a mass of $\approx 10 \text{ mg}$ were encapsulated in small $20\text{-}\mu\text{L}$ - (PLLA) or large $40\text{-}\mu\text{L}$ -aluminum pans (PDLLA) and rapidly cooled from $220 \text{ }^\circ\text{C}$ to $-50 \text{ }^\circ\text{C}$, in order to suppress crystallization in case of PLLA. To obtain the temperature dependence of the heat capacity, samples were heated using a rate of 20 K min^{-1} , with the recorded heat-flow-rate curves corrected for instrumental asymmetry and calibrated using sapphire as standard. A total of seven (PLLA) or three (PDLLA) samples was analyzed, yielding averages of 0.54 ± 0.03 and $0.55 \pm 0.01 \text{ J g}^{-1} \text{ K}^{-1}$, respectively, as heat-capacity increment at T_g . Besides analysis of the heat-capacity step of fully amorphous samples at T_g , DSC was also used to confirm mass-normalized enthalpies of melting obtained by FSC. Samples with a mass of $\approx 5 \text{ mg}$ were encapsulated in $20\text{-}\mu\text{L}$ -aluminum pans and heated after isothermal crystallization at a rate of 10 K min^{-1} , to obtain enthalpies of melting. Further details about the crystallization route are provided below.

Small-Angle X-Ray Scattering: Small-angle X-ray scattering (SAXS) data were collected using monochromatic X-rays with a wavelength of 0.154 nm , and a Kratky compact camera (Anton Paar GmbH, Graz, Austria), operated in vacuum and equipped with a focusing X-ray optics (AXO Dresden GmbH, Dresden, Germany) and a 1D position-sensitive Mythen2 R 1K detector (Dectris AG, Baden, Switzerland). For SAXS analysis, film samples with a thickness of $\approx 220 \text{ }\mu\text{m}$ were prepared by compression molding at $220 \text{ }^\circ\text{C}$, using a LOT QD (Darmstadt, Germany) hydraulic press in combination with a film-pressing tool and temperature control (Specac Ltd., Orpington, UK). Before compression molding, the as-received pellets were dried at $90 \text{ }^\circ\text{C}$ overnight. The films, sandwiched between Teflon layers, were quickly transferred from the die with a temperature of $220 \text{ }^\circ\text{C}$ to an oven (Mettler-Toledo, Greifensee, Switzerland), preheated to $140 \text{ }^\circ\text{C}$, and crystallized for different time. After crystallization, the samples were quenched to room temperature, in order to suppress continuation of crystallization on cooling. All SAXS measurements were quantitatively analyzed based on modeling the interface distribution function,^[42,43] providing average thicknesses of crystal lamellae d_c and interlamellar amorphous regions d_a . With these parameters the linear crystallinity can be determined as $X_{c, \text{SAXS}} = d_c / (d_c + d_a)$. Further details of the evaluation of SAXS data are provided in the Supporting Information S1.

3. Results and Discussion

3.1. FSC Analysis of the Bulk Enthalpy of Melting of α -Crystals of PLLA

Figure 1 shows the thermal protocol for evaluation of the bulk enthalpy of melting of α -crystals of PLLA formed at $140 \text{ }^\circ\text{C}$. Direct melt-crystallization of PLLA at $140 \text{ }^\circ\text{C}$ in an FSC, due to the small sample size and low crystal-nucleation rate,^[44,45] is slow and nonreproducible regarding the kinetics. For this reason, the crystallization step (red segment) was preceded by an annealing step at $60 \text{ }^\circ\text{C}$, to allow formation of nuclei for 300 s . These nuclei were then slowly transferred to the crystallization temperature,

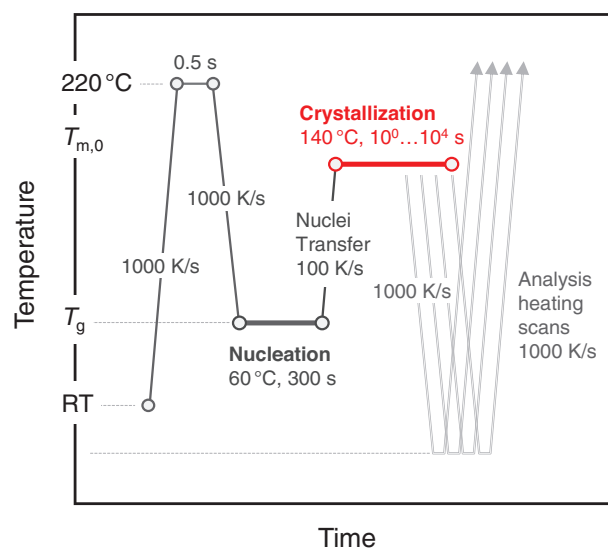


Figure 1. Thermal protocol for analysis of the bulk enthalpy of melting of α -crystals of PLLA. The relative positions of the equilibrium melting temperature ($T_{m,0}$), room temperature (RT), and glass transition temperature (T_g) are indicated.

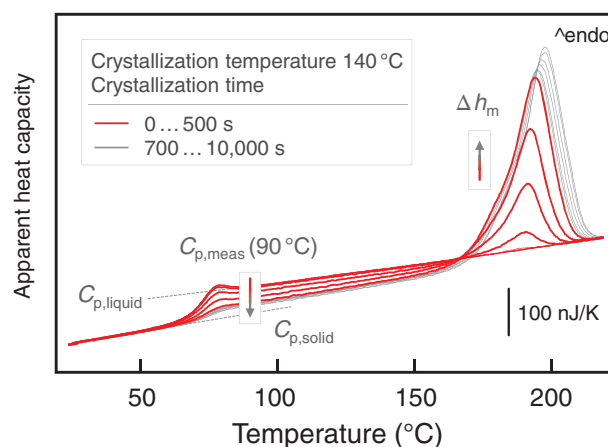


Figure 2. FSC heating scans of PLLA obtained after crystallization at $140 \text{ }^\circ\text{C}$ for different time, recorded using a rate of 1000 K s^{-1} . Red and gray coloring of curves indicate crystallization-time ranges of primary and secondary crystallization, respectively, as derived from the slowing down of the crystallization kinetics on increasing the crystallization time, quantified below with Figure 3.

with the low transfer-heating rate of 100 K s^{-1} minimizing loss of nuclei by disordering.^[46,47] The kinetics of cold-crystallization at $140 \text{ }^\circ\text{C}$ after such nucleation step is highly reproducible as will be outlined below. Crystallization was performed up to $10\,000 \text{ s}$, however, interrupted at predefined times to obtain samples of different crystallinity or enthalpy of crystallization/melting. After the crystallization step, the sample was rapidly cooled to $-60 \text{ }^\circ\text{C}$ using a rate of 1000 K s^{-1} and reheated at identical rate for observation of the heat capacity at $90 \text{ }^\circ\text{C}$ and the enthalpy of melting at T_m (see gray lines, labeled “Analysis heating scans”).

Figure 2 shows example-FSC-heating curves of PLLA, which was crystallized according to the thermal protocol of Figure 1 at $140 \text{ }^\circ\text{C}$. The various curves represent different crystallization

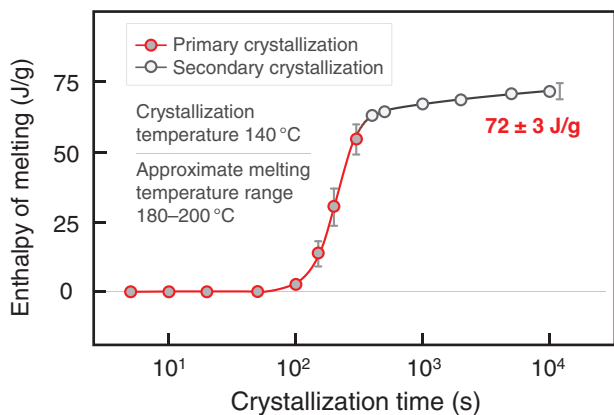


Figure 3. Enthalpy of melting of crystals of PLLA formed at 140 °C and melting between, roughly, 180 and 200 °C as a function of the crystallization time. Data are averages of six measurements with error bars shown only if exceeding the symbol size. Red/dark-gray and black/light-gray data points indicate crystallization-time ranges of primary and secondary crystallization, respectively.

times between 1 and 10 000 s, with red and gray coloring indicating time ranges of primary and secondary crystallization, respectively. All curves show on heating the heat-capacity step due to the glass transition at ≈ 70 °C, which is slightly higher compared to the often reported value of 60 °C, due to the high cooling rate in the preceding cooling scan and the heating scan, and possible thermal lag during heating.^[38,48] Then, on further heating, an endothermic peak caused by melting of crystals formed at the crystallization temperature is detected. Melting begins slightly above the crystallization temperature and stretches over a wide temperature range, depending on the crystallization time. With increasing crystallization time, as indicated by the two vertical arrows, the heat capacity ($C_{p,meas}$) at a temperature slightly higher than T_g , at 90 °C, decreases and the melting-peak area/enthalpy of melting (Δh_m) increases.

Figure 3 shows the enthalpy of melting of crystals of PLLA as a function of the crystallization time, with the crystals grown at 140 °C and melting between 180 and 200 °C. Data are averages of six measurements with a typical error bar shown for selected data points only. Red/dark-gray and black/light-gray data points indicate crystallization-time ranges of primary and secondary crystallization. Most important is the observation of a quasi-final value of the enthalpy of crystallization of 72 J g⁻¹ after crystallization/annealing PLLA for 10 000 s. We consider this value as quasi-final only, as there is expected a further minor increase on extension of annealing due to secondary crystallization, following a logarithmic time dependence.^[49,50]

A major experimental challenge to observe the specific, sample-mass-normalized enthalpy of melting of 72 J g⁻¹ after long-term crystallization at 140 °C is the determination of the mass of FSC samples. Due to their low size, a direct measurement using a balance is impossible, requiring indirect estimation.^[51] In the present work, the sample-mass estimation is based on the comparison of the measured absolute heat-capacity step at T_g of a fully amorphous sample (in units of J K⁻¹) with the expected, mass-normalized heat-capacity step (in units

of J g⁻¹ K⁻¹). Regarding the latter, the initially suggested value of 0.608 J g⁻¹ K⁻¹ (= 43.8 J mol⁻¹ K⁻¹/72.06 g mol⁻¹),^[15,52] based on a detailed analysis/computation of the temperature-dependence of the heat capacity of solid and liquid PLLA, is not unequivocally agreed upon in the literature,^[20,53–58] where often lower values between 0.49^[56] and 0.57 J g⁻¹ K⁻¹^[56] are reported. Own measurements performed on the specific PLLA grade used in this work, and non-crystallizable PDLLA, suggest a value of 0.54(5) J g⁻¹ K⁻¹ at 60.5 °C that then has been used to estimate the mass of the FSC samples. Here, the slightly increased glass transition temperature in FSC analyses (being observed at a temperature ≈ 10 K higher than in DSC analyses) is accounted for by a minor correction of the heat-capacity step of 0.54(5) J g⁻¹ K⁻¹ at 60.5 °C to 0.52(7) J g⁻¹ K⁻¹, related to the nonparallel temperature-dependencies of the heat capacity of fully liquid and solid PLLA.^[15]

Additionally, the correctness of the determination of the mass of FSC samples is confirmed by independent DSC analysis of enthalpies of melting of PLLA crystals formed at 140 °C. Crystallization of PLLA at 140 °C for 3 h (10 800 s) in the DSC yielded a value of 68 J g⁻¹. The small discrepancy between the enthalpies of melting of 68 and 72 J g⁻¹, observed after crystallization at 140 °C in the DSC and FSC, respectively, may be attributed to different nucleation pathways. In case of analysis of high-temperature crystallization of PLLA in the DSC, an additional low-temperature nucleation step as in FSC analyses is not needed, due to the much larger sample size (compare 10⁻¹ μ g (FSC) and 10⁴ μ g (DSC)). This notwithstanding, exact matching of nuclei numbers in FSC and DSC analyses is impossible, causing different overall crystallization rates and therefore also different crystallinity values after a predefined crystallization time. A further reason of the slightly lower enthalpy of melting in DSC experiments may be the lower melting temperature of about only 180 °C, in comparison to ≈ 190 °C when using FSC. According to Kirchhoff's law of thermochemistry, this leads to a decrease of the bulk enthalpy of melting via Equation (1):^[59]

$$\Delta h_{m,100}(T_2) = \Delta h_{m,100}(T_1) + \Delta c_p \times (T_2 - T_1) \quad (1)$$

Here, Δc_p is the average difference of the heat capacities of the crystalline and liquid phases in the temperature range of interest, between T_1 [$= T_{m,DSC}$] and T_2 [$= T_{m,FSC}$]. As such, a decrease of T_m by 10 K [$= T_2 - T_1$] causes a lowering of the bulk enthalpy of melting of ≈ 3.4 J g⁻¹ when using a Δc_p -value of 0.34 J g⁻¹ K⁻¹ at 458 K, as suggested in the literature.^[15]

Figure 4 shows the correlation between the decrease of the specific heat capacity of PLLA at 90 °C [$= c_{p,meas} - c_{p,liquid}$] and the enthalpy of melting of crystals formed at 140 °C and melting at 180–200 °C (Δh_m). Measurements have been repeated six times, using different samples, indicated by different symbols. In analogy to Figure 3, data obtained during primary and secondary crystallization, are represented by red/dark-gray and black/light-gray symbols, respectively. The data of Figure 4 reveal the expected decrease of the heat capacity during the crystallization process, due to the increase of the solid fraction. Estimation of the solid fraction after completion of primary crystallization and extended secondary crystallization yields values of 56% and 72%, respectively.

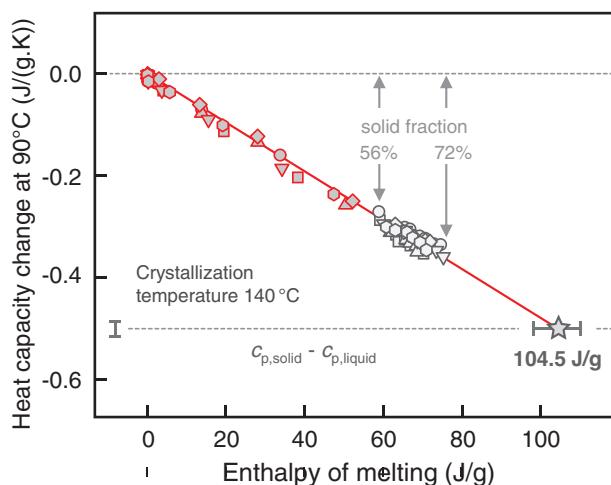


Figure 4. Change of the specific heat capacity of PLLA at 90 °C ($= c_{p,meas} - c_{p,liquid}$) as a function of the enthalpy of melting of crystals formed at 140 °C and melting between 180 and 200 °C (Δh_m). Different symbols represent analyses of different samples, for the sake of obtaining information about measurement errors. Red/dark-gray and black/light-gray symbols indicate the assignment of data to primary and secondary crystallization, respectively. The red line is drawn to guide the eye. The heat-capacity difference between solid and liquid PLLA ($= c_{p,solid} - c_{p,liquid} = -0.500 \pm 0.016 \text{ J g}^{-1} \text{ K}^{-1}$) at 90 °C is indicated with the bottom horizontal dash line and is an average of all measurements performed, with the standard deviation indicated to the left of the line. This error represents the uncertainty regarding the extrapolation of $c_{p,solid}$, measured below T_g , to 90 °C. Furthermore, the various data sets were fitted individually to yield different values of $\Delta h_{m,100}$ ($T = 190 \text{ °C}$), with the resulting standard deviation provided with the horizontal error bar.

The decrease of the heat capacity with increasing enthalpy of melting is linear, indicating either the validity of a two-phase structure composed of solid crystals and liquid amorphous phase at the analysis temperature of 90 °C, or the presence of a three-phase structure, composed of solid crystals, a solid/vitrified RAF (with $c_{p,solid} = c_{p,glass} = c_{p,crystal}$) and liquid amorphous phase; in the latter case, the vitrified RAF would linearly increase with the crystallinity. A parallel increase of the RAF and of the crystal fraction, regardless whether crystals form during primary crystallization, or whether the crystallinity increases during secondary crystallization, seems unlikely, considering the qualitatively different semicrystalline morphologies developing at these stages of the crystallization process. It will be shown below that during isothermal crystallization at 140 °C, and subsequent cooling of the system to the temperature of analysis the solid fraction (90 °C), indeed, RAF formation/vitrification is absent. As such, the various data sets of Figure 4 were individually fitted with a linear function (Equation 2), allowing their extrapolation toward the heat capacity of fully solidified PLLA ($c_{p,solid}$) and estimation of $\Delta h_{m,100}$ ($T = 190 \text{ °C}$), to be $104.5 \pm 6.0 \text{ J g}^{-1}$ (see star symbol):

$$c_{p,meas} - c_{p,liquid} = \Delta h_m / \Delta h_{m,100} \times (c_{p,solid} - c_{p,liquid}) \quad (2)$$

The left part of Equation (2) represents the ordinate in Figure 4 that is plotted as a function of Δh_m . Note again, all c_p -values are obtained at 90 °C while enthalpies of melting hold for the melting temperature range from 180 to 200 °C.

3.2. Absence of RAF Formation/Vitrification

In the present work, crystals were formed at 140 °C while the crystal fraction was analyzed at 90 °C. As outlined above, correlation between the heat-capacity change at 90 °C and the crystal fraction relies on the presence of a two-phase structure, that is, absence of a vitrified RAF at the temperature of analysis the crystal fraction (90 °C). In general, RAF formation and vitrification may occur at different temperatures. In other words, crystallization at 140 °C may cause formation of RAF at the crystallization temperature, which, however, may only vitrify during subsequent cooling.^[29,30] Though this scenario is not unequivocally discussed in the literature, contrasting observations suggesting vitrification of RAF at T_c ,^[60–63] in this work, RAF vitrification during cooling is not a priori ruled out. As such, the following cases, leading to formation of a three-phase structure at 90 °C, will be discussed: a) RAF forms and vitrifies at T_c , b) RAF forms at T_c and vitrifies on cooling to 90 °C, and c) RAF forms and vitrifies on cooling to 90 °C due to continuation of crystallization; worth noting, detection of un-vitrified RAF, if possible at all, is beyond the scope of the present work and only absence of vitrification at temperatures above 90 °C is of interest here.

Absence of vitrification of RAF during isothermal crystallization at 140 °C is suggested by SAXS analysis of the evolution of the crystal thickness and linear crystallinity during extended annealing/isothermal secondary crystallization, while absence of vitrification of RAF during the transfer of samples of different crystallinity to 90 °C is supported by analysis of the temperature-dependence of the heat capacity between 90 and 140 °C during fast cooling/heating, using FSC. The corresponding experimental evidences are described in the following two sections.

3.2.1. SAXS Analysis of PLLA Crystallized at 140 °C

SAXS data were collected on samples of PLLA crystallized for different time at 140 °C and subsequently quenched to ambient temperature, to avoid continuation of crystallization during cooling. In any case, only samples with completed primary crystallization were analyzed, that is, focus is the change of structure during isothermal secondary crystallization at 140 °C. Completion of primary crystallization is assured by parallel analysis of the enthalpy of melting by DSC and of the micrometer-scale structure using polarized-light optical microscopy (POM); regarding the latter, see Figure S2, Supporting Information. As such, by using POM, presence of a space-filled spherulitic superstructure is evidenced for all samples analyzed by SAXS. Figure 5 shows in the bottom part enthalpies of melting of PLLA films as a function of the time of crystallization at 140 °C, revealing begin of crystallization after ≈ 600 s and completion of the primary crystallization process, as judged by the distinct change of the kinetics of crystallization, after ≈ 5000 s. Continuation of the increase of the enthalpy of melting on annealing samples longer than 5000 s suggests secondary crystallization, however, with the exact mechanism not yet reported in the literature. The center part of Figure 5 shows the evolution of the lamellar thickness d_c during secondary crystallization of PLLA at 140 °C, as obtained by SAXS. As such, after completion of primary crystallization, d_c is ≈ 15 nm and increases to ≈ 17 nm after extended annealing for 604 800 s (= 7 days), that

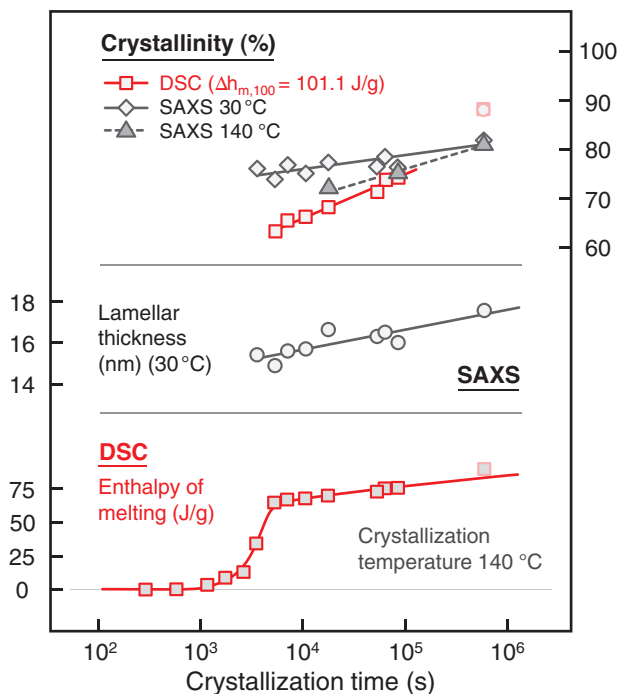


Figure 5. Enthalpy of melting of crystals of PLLA formed at 140 °C and melting at 180 °C (peak temperature), measured by DSC (bottom data), thickness of crystal lamellae of PLLA formed at 140 °C and measured by SAXS at 30 °C (center data), and linear SAXS-crystallinities (measured at 30 and 140 °C) and DSC crystallinity (top data) as a function of the crystallization time.

is, by $\approx 15\%$ within the investigated crystallization-time range of 1 week. Such increase of the lamellar thickness is common for so-called crystal-mobile polymers, that is, semicrystalline polymers with an α_c -relaxation,^[64] caused by mobile conformational defects in the crystals. The dynamics of these defects in PLLA was previously characterized.^[65] Specifically, the increase of the lamellar thickness is also indicative for the absence of a glassy amorphous layer at the fold-surface of the lamellae, that is, absence of a vitrified RAF at the crystallization temperature, as in such case longitudinal crystal growth is assumed restricted. The increase of the crystal thickness during isothermal annealing at the temperature of primary crystallization is confirmed in an independent study, reporting values of the lamellar thickness of 13.9 and 16 nm after melt-crystallization of PLLA at 140 °C for 90 and 600 min, respectively,^[66] suggesting lamellar thickening as a valid secondary-crystallization process for PLLA. Worth noting that a similar crystal thickness of close to 16 nm was observed in PLLA cold-crystallized at 140 °C for 60 min.^[67] Furthermore, the observed increase of the lamellar thickness during secondary crystallization also shows up by an increase of the melting temperature by ≈ 3 K, from 178 °C after crystallization for 5400 s (end of primary crystallization) to ≈ 181 °C (after long-term annealing for 1 week). Such increase is in accord with the Gibbs-Thomson equation, relating the melting temperature of crystals with their size,^[68] and has also been observed in the FSC heating scans of Figure 2; note that in the latter case the melting peaks, throughout, are shifted to higher temperature compared to the DSC experiment, caused by faster heating.

Though not primary focus of the SAXS experiment, initially intended for proving lamellar thickening only, analysis of the linear crystallinity, consistently, both in the literature,^[15,67,69] and here, yields values well above 60–70%, depending on the crystallization time and analysis temperature; note that the bulk crystallinity may be lower than the linear crystallinity, with the difference, however, being negligible, as outlined below. The upper part of Figure 5 shows the evolution of the crystallinity with the time of secondary crystallization at 140 °C, measured by SAXS at 30 °C and, for selected samples, at 140 °C (gray diamond symbols/solid line and triangles/dash line, respectively), and by DSC (red symbols per line). The latter values were calculated using a bulk enthalpy of melting of 101.1 J g⁻¹, as estimated by Kirchoff's law, described above. In both cases, DSC- and SAXS-analyses, the crystallinity increases with the time of secondary crystallization, due to lamellar thickening. The coincidence of SAXS and DSC crystallinities (gray triangles and red squares, respectively) suggests furthermore that the linear SAXS crystallinity must be close to the bulk crystallinity, which also would consider amorphous fractions outside of lamellar stacks. Comparing DSC crystallinities with the crystallinity calculated from SAXS data obtained at 30 °C, it is observed that the DSC crystallinities are slightly lower, in particular at shorter crystallization time; this observation is confirmed by independent analysis of samples crystallized in the DSC for up to 5 h (not shown since these samples were not analyzed by SAXS). The DSC crystallinity of the sample crystallized for 1 week, measured on two independent samples to assure reproducibility, in contrast, exceeds the SAXS crystallinity, and seems off the trend. For this reason, these data points are drawn in light red, indicating the need for further investigations, in particular since the crystallinity seems unreasonable high, being close to 90%.

In order to shed more light on the observed difference between the SAXS-crystallinity measured at 30 °C and DSC crystallinity at short secondary-crystallization times, SAXS data were collected also at 140 °C for selected samples (gray triangles, dash line). In that case, the initially quenched samples were stepwise heated to 140 °C, to monitor the change of the linear SAXS-crystallinity during slow heating (not shown). Comparing SAXS-crystallinities observed at 30 and 140 °C reveal almost identical values for long crystallization time while for shorter crystallization time the crystallinity at 140 °C is lower than at 30 °C. With the assumption that prior quenching the sample from 140 to 30 °C suppressed slow irreversible formation of new crystals as well as slow irreversible lamellar thickening during cooling, evidenced below, the decrease of the SAXS-crystallinity on reheating to 140 °C indicates reversible surface melting of lamellae, as discovered and investigated long ago by dedicated experiments using SAXS and temperature-modulated DSC for several polymers.^[70–73] Such reversible melting process represents a local equilibrium at the fold-surface of lamellar crystals. It involves a force balance between the recovery tendency of the stretched loops (on heating) and a thickening tendency of the lamellae (on cooling).^[71] Furthermore, it is expected to not show a kinetics, thus it also occurs during quenching, as in the present case. Since the DSC analysis of the crystallinity is based on the irreversible melting process occurring above the crystallization temperature, such reversible increase of the crystallinity during cooling is not accounted for. Obviously, reversible crystallization (on cooling)

and melting (on heating) is less pronounced, or even completely absent in case of highly crystalline samples containing rather thick lamellae and low amount of interlamellar amorphous structure, causing increasing constraints for further (reversible and irreversible) thickening. This view would support the agreement of SAXS and DSC crystallinities in case of the long-term annealed sample.

In summary, SAXS analysis of the evolution of the lamellar thickness and linear crystallinity during long-term annealing of PLLA at the temperature of primary crystallization of 140 °C suggests lamellar thickening as a valid mechanism of secondary crystallization and strongly supports the view of absence of a vitrified RAF at the crystal basal planes at the crystallization temperature. Both SAXS and DSC suggest crystallinities above 70%, however, with the minor mismatch observed requiring further experimentation, including estimation of bulk SAXS crystallinities (evidencing absence of a large amorphous fraction outside of lamellar stacks) and in-depth analysis of the temperature-dependence of the lamellar thickness and long period (providing information about reversible surface crystallization and melting).

3.2.2. Absence of RAF Vitrification on Fast Cooling Semicrystalline PLLA, Crystallized at 140 °C, to 90 °C

SAXS provided evidence that there does not exist a glassy amorphous fraction at the lamellae basal planes, neither at the end of primary crystallization nor after secondary crystallization for 1 week. However, this experiment cannot exclude vitrification of an amorphous fraction on cooling the system to the C_p -analysis-temperature of 90 °C. Therefore, additional attempts were made to prove/disprove such vitrification of an amorphous fraction during cooling.

In a first experiment, we followed the idea of detection mobility of amorphous chain segments at the interface of crystals formed at 140 °C and the surrounding amorphous phase. PLLA was crystallized at 140 °C for 500 s after nucleation at 60 °C for 300 s in the FSC (see also Figure 3), allowing completion of the primary crystallization process, and was then annealed at lower temperatures between 80 and 130 °C for 10 000 s. After the annealing step, samples were heated in the FSC to detect the changes of structure. In particular, it was attempted to show that crystals formed at higher temperature of 140 °C are subject of stabilization/lamellar thickening during low-temperature annealing, based on a recent study of crystal stabilization of poly(butylene terephthalate) (PBT).^[74] In that study, it was illustrated that annealing of crystals grown at higher temperature stabilize such to exhibit a higher melting temperature after the low-temperature annealing event, with the stabilization process becoming less distinct with decreasing annealing temperature/increasing difference of the temperatures of primary crystallization and annealing. For PLLA of the present work, a similar behavior is detected, that is, lamellae formed at 140 °C stabilize on subsequent annealing at lower temperature, causing an increase of their melting temperature, as discussed above for the isothermal secondary crystallization experiment.

An example of such an experiment is provided with **Figure 6**, showing FSC heating scans of PLLA crystallized for 500 s at 140 °C (red) and of PLLA that was additionally annealed at 100 °C for 10, 100, and 1000 s (gray solid lines), and for 10 000 s (blue). The

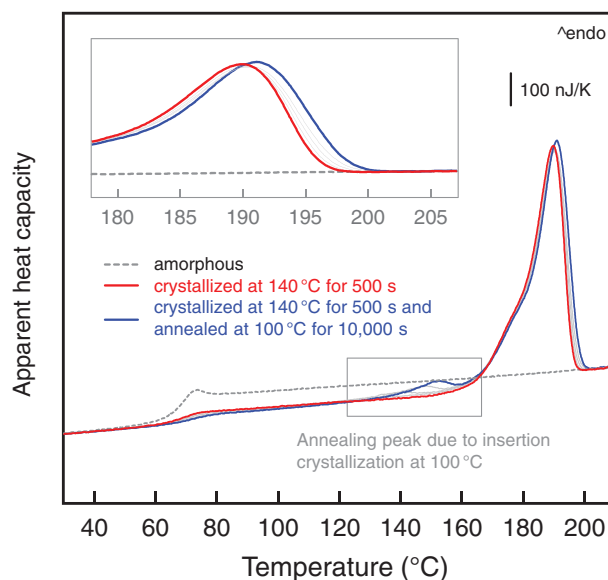


Figure 6. FSC heating scans of PLLA obtained after crystallization at 140 °C for 500 s (red), crystallization at 140 °C for 500 s and subsequent annealing for 10, 100, 1000 s (gray), and 10 000 s (blue) at 100 °C. The dash line represents a heating scan obtained on a fully amorphous sample. The heating rate was 500 K s⁻¹. The inset shows the main melting peak at an enlarged scale.

dash line represents an FSC scan obtained on fully amorphous PLLA. Annealing at 100 °C causes formation of smaller crystals than grown at 140 °C, characterized by a lower melting temperature, as discussed in detail in a recent study about insertion crystallization induced annealing peaks in PLLA (see also boxed part of the FSC curves).^[32] Simultaneously low-temperature annealing leads to a shift of the melting temperature of crystals formed at 140 °C, which is shown enlarged in the inset. For given conditions of the high-temperature crystallization process (here 140 °C, 500 s) and given low-temperature annealing time, the shift of the melting temperature decreases with decreasing annealing temperature. While annealing at 100 °C still allowed detection of a distinct shift of the melting temperature of lamellae formed at 140 °C by more than 1 K, annealing at 90 °C, that is, 50 K below the primary crystallization process, measurable stabilization of lamellae formed at 140 °C was close to the detection limit. Nevertheless, the observation of a shift of the melting temperature of crystals formed at 140 °C, due to annealing at lower temperature, at least supports the view that these lamellae are subject of structural reorganization also at temperatures lower than their formation. Such reorganization is assumed requiring mobility of chain segments at the crystal surfaces, which may not be evident if surrounded by a glassy RAF.

Furthermore, worth noting, a rough estimate of the link between the increase of the lamellar thickness and the corresponding increase of the melting temperature, using the Gibbs-Thomson equation, provided information that an increase of the lamellar thickness by 1 nm causes a shift of T_m by ≈ 1 K.^[75] This estimate is based on using values of the fold-surface free energy, bulk enthalpy of melting, and equilibrium melting temperature of 61×10^{-3} J m⁻², 111×10^6 J m⁻³, and 480 K, respectively, as suggested in the literature.^[76] Such increase of the lamellar

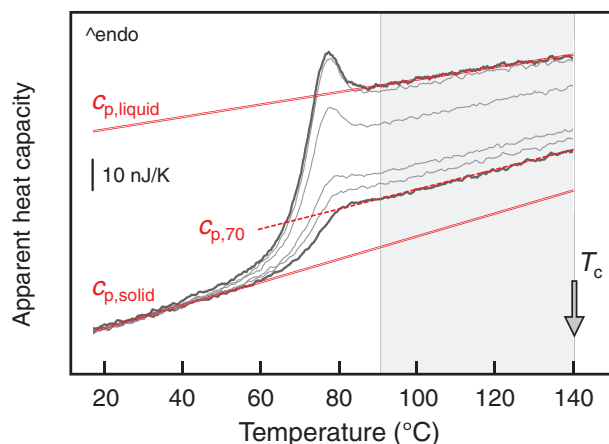


Figure 7. FSC heating curves of PLLA isothermally crystallized for different time at 140 °C (0, 100, 200, 300, 500, and 10 000 s, from top to bottom) and subsequently cooled at 1000 K s⁻¹ to the heating-scan-start temperature of -60 °C (see the complete thermal protocol in the left part of Figure 1). Scans were recorded using a heating rate of 1000 K s⁻¹, and show details in the temperature range between the glass transition temperature T_g and the crystallization temperature T_c ; the full temperature range was shown with the bottom curve set in Figure 2. The solid red lines represent the heat capacities of liquid and solid PLLA, and the dashed red line the heat capacity of PLLA containing 70% solid structure.

thickness by 1 nm requires the transition of an amorphous layer with a thickness of about the length of a full molecular repeat unit, adopting a helical chain conformation, into the crystalline state at the crystal fold surface; in orthorhombic α -crystals, forming at 140 °C, molecular chains adopt a 10/3 helical conformation, to yield a fiber period of around 2.8 nm, involving three chain repeat units.^[22,77–79]

A further approach of proving/disproving RAF-formation and vitrification includes an inspection of the FSC-heating curves recorded after crystallization PLLA at 140 °C for different periods of time and subsequent fast cooling at a rate of 1000 K s⁻¹ to the scan-start temperature of -60 °C. **Figure 7** shows such heating scans for samples crystallized at 140 °C for 0, 100, 200, 300, 500, and 10 000 s (from top to bottom), with the complete temperature–time profile of the experiment shown in Figure 1. The heating scans are presented in a limited temperature-range only, allowing discussion of the temperature-dependence of the heat capacity between the glass transition temperature T_g and the crystallization temperature T_c . The solid red lines represent the heat capacities of liquid and solid PLLA, and the dashed red line the (hypothetical) heat capacity of PLLA containing 70% solid structure, calculated as mass-weighted sum of the heat capacities of fully liquid and solid PLLA, assuming a two-phase structure.

Above it is shown that crystallization of PLLA at 140 °C permits lamellar thickening after completing primary crystallization, proving absence of a glassy amorphous layer at the lamellae fold surface at this temperature. As such, the assumption of a two-phase structure at the C_p -analysis temperature of 90 °C would only be invalid if part of the amorphous phase vitrifies during cooling the system from T_c to T_g , and correspondingly devitrifies on heating in the same temperature range (see the gray shaded area in Figure 7). However, the FSC-heating scans, in contrast, suggest absence of such devitrification process since

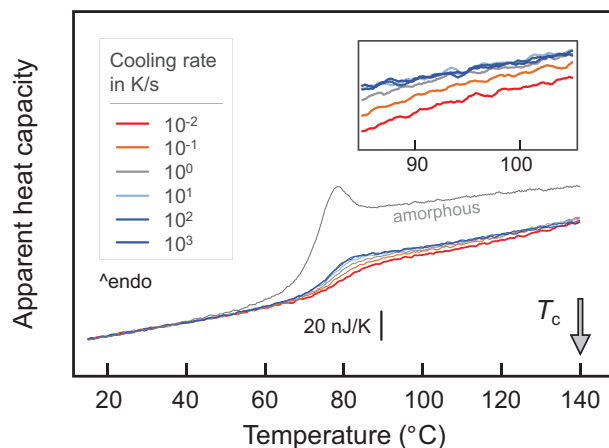


Figure 8. FSC heating curves of PLLA isothermally crystallized at 140 °C for 500 s, after prior nucleation at 60 °C for 300 s, and then cooled at different rate between 0.01 and 1000 K s⁻¹ to 80 °C, as indicated in the legend. Then the samples were further cooled to below the glass transition temperature, and re-heated, both at a rate of 1000 K s⁻¹. The inset shows FSC curves at an enlarged scale between 85 and 105 °C, and the gray curve was obtained on a fully amorphous sample.

the measured curves, regardless the crystallization time, do not reveal any thermal transition and prove instead constant liquid–solid ratio in the temperature range of interest, as, e.g., concluded from the coincidence of measured heat-capacity data of the sample crystallized for 10 000 s (bottom curve) with the corresponding heat-capacity baseline (red dashed line) of PLLA containing 70% solid structure. As such, with the knowledge of absence of a glassy amorphous fraction, the solid fraction equals the crystal fraction in the sample.

Worth noting that we are aware of studies suggesting for samples crystallized at 140 °C, or even higher temperature, vitrification of about half of the amorphous phase on slow cooling at 2 K min⁻¹ in the temperature range between T_c and the glass transition temperature T_g of the bulk amorphous phase.^[29,30] We explain this observation by slow secondary crystallization/formation of new crystals in the temperature range between T_c and T_g . Such secondary crystallization is expected occurring during slow but not fast cooling, based on a recent analysis of the time-dependence of generation of annealing peaks.^[32] This expectation has been confirmed by inspection of FSC heating scans obtained on samples cooled at different rate after primary crystallization at 140 °C for 500 s, preceded by a nucleation step at 60 °C for 300 s (see also Figure 1), as shown in **Figure 8**. The cooling rate was varied between 0.01 and 1000 K s⁻¹, applied within the temperature range from 140 to 80 °C. After cooling the samples at a specific rate to 80 °C, further cooling to below T_g was performed for all samples at 1000 K s⁻¹, to assure an identical glass-relaxation history; vitrification of the amorphous phase at different cooling rates produces in the subsequent heating scan enthalpy-recovery peaks of different area,^[80,81] disturbing analysis of the heat capacity at slightly higher temperature.

The data of Figure 8 show a systematic lowering of the (apparent) heat capacity at temperatures lower than the temperature of primary crystallization of 140 °C if the cooling rate is lower than ≈ 10 K s⁻¹; faster cooling has an only negligible effect on the FSC

curves. Such lower heat capacities are caused by an increase of the crystallinity due to non-isothermal secondary crystallization during prior cooling, perhaps in combination with a partial vitrification of an amorphous fraction. It is important to note that any RAF formation/vitrification is then based on crystals formed during cooling but not on crystals formed at 140 °C, as in the latter case a vitrification could not be suppressed by fast cooling. A deeper investigation about possible RAF-formation and vitrification during slow cooling, however, is clearly beyond the scope of this study, as it is provided in the literature.^[29,30]

4. Conclusions

Reports about the bulk enthalpy of melting of crystals of PLLA in the literature scatter over a wide range, limiting a reliable determination of the crystallinity by calorimetry. For this reason, in this work, the bulk enthalpy of melting of α -crystals of PLLA has been re-determined using FSC, by analysis of the relationship between the specific heat capacity of semicrystalline samples at a temperature between the crystallization temperature T_c and the glass transition temperature T_g of the bulk amorphous phase on one side, and the corresponding enthalpy of melting on the other side. Extrapolation of this relationship toward the specific heat capacity of fully solid PLLA yields the bulk enthalpy of melting, with the presumption that samples only contain crystals and liquid amorphous phase at the temperature of analysis of the heat capacity. Going beyond prior studies in this field, great effort was undertaken to fulfill and prove the precondition of absence of a vitrified RAF at the temperature of analysis the solid fraction after specific crystallization experiments. In detail, the following conclusions were derived:

- (a) The bulk enthalpy of melting of α -crystals of PLLA, formed at 140 °C and melting between 180 and 200 °C is 104.5 ± 6.0 J g⁻¹, being close to values suggested by Prud'homme and Strobl.^[13,16]
- (b) Crystallization at 140 °C yields a lamellae with a thickness of ≈ 15 nm at the end of the primary-crystallization stage that significantly thicken during isothermal secondary crystallization at identical temperature. The observed lamellar thickening proves the absence of a glassy amorphous layer at the fold surface of the lamellae.
- (c) Thickening/stabilization of lamellae formed at 140 °C continues at lower temperature, however, fades with decreasing temperature.
- (d) Cooling PLLA, containing lamellae formed at 140 °C, faster than ≈ 10 K s⁻¹ suppresses non-isothermal secondary crystallization and vitrification of parts of the amorphous phase at temperatures above T_g of the bulk amorphous phase.
- (e) The crystallinity of isothermally at 140 °C crystallized PLLA, not containing crystals formed during cooling, estimated by SAXS and calorimetry, yield similar values, exceeding 70% after long-term crystallization. The close though not perfect coincidence of the linear crystallinity, determined by SAXS, and the enthalpy-based crystallinity suggests presence of space-filling homogeneous lamellar stacks.

Supporting Information

Supporting Information is available from the Wiley Online Library or from the author.

Acknowledgements

K.J., M.D., and R.A. thank the Deutsche Forschungsgemeinschaft (DFG) (grants AN 212/20 and 26) for financial support, and C.S. is grateful for a grant by the Ministry of Education and Science of the Russian Federation (grant 14.Y26.31.0019). T.T.A. and Q.Y. acknowledge funding by the Deutsche Forschungsgemeinschaft (DFG) – Project-ID 189853844 – TRR 102. The authors thank Corbion for providing the polymer and Aaron Miller and Venkata Vulchi for performing SAXS-measurements.

Open access funding enabled and organized by Projekt DEAL.

Conflict of Interest

The authors declare no conflict of interest.

Data Availability Statement

The data that support the findings of this study are available from the corresponding author upon reasonable request.

Keywords

bulk enthalpy of melting, crystallinity, fast scanning chip calorimetry (FSC), poly(L-lactic acid) (PLLA), small-angle X-ray scattering (SAXS)

Received: February 17, 2022

Revised: March 19, 2022

Published online:

- [1] T. A. Osswald, G. Menges, *Materials Science of Polymers for Engineers*, Hanser, München, **2012**.
- [2] S. Fakirov, *Fundamentals of Polymer Science for Engineers*, Wiley, Weinheim, **2017**.
- [3] D. Mileva, D. Tranchida, M. Gahleitner, *Polym. Cryst.* **2018**, *1*, e10009.
- [4] S. Kavesch, J. M. Schultz, *Polym. Eng. Sci.* **1969**, *9*, 331.
- [5] A. P. Gray, *Thermochim. Acta* **1970**, *1*, 563.
- [6] Y. Kong, J. N. Hay, *Polymer* **2002**, *43*, 3873.
- [7] J. Runt, M. Kanchanasopa, Crystallinity Determination, In: *Encyclopedia of Polymer Science and Technology*, Wiley, **2002**.
- [8] B. Wunderlich, *Thermal analysis of polymeric materials*, Springer, Berlin, **2005**.
- [9] M. L. Di Lorenzo, R. Androsch, *Industrial applications of poly(lactic acid)*, Springer, Cham, **2018**.
- [10] E. W. Fischer, H. J. Sterzel, G. Wegner, *Kolloid-Z. Z. Polym.* **1973**, *251*, 980.
- [11] D. K. Gilding, A. M. Reed, *Polymer* **1979**, *20*, 1459.
- [12] K. Jamshidi, S.-H. Hyon, Y. Ikada, *Polymer* **1988**, *29*, 2229.
- [13] J.-R. Sarasua, R. E. Prud'homme, M. Wisniewski, A. Le Borgne, N. Spassky, *Macromolecules* **1998**, *31*, 3895.
- [14] T. Miyata, T. Masuko, *Polymer* **1998**, *39*, 5515.
- [15] M. Pyda, R. C. Bopp, B. Wunderlich, *J. Chem. Thermodyn.* **2004**, *36*, 731.
- [16] T.-Y. Cho, G. Strobl, *Polymer* **2006**, *47*, 1036.

- [17] P. Badrinarayanan, K. B. Dowdy, M. R. Kessler, *Polymer* **2010**, *51*, 4611.
- [18] C.-Y. Chen, C.-F. Yang, U.-S. Jeng, A.-C. Su, *Macromolecules* **2014**, *47*, 5144.
- [19] M. C. Righetti, M. Gazzano, M. L. Di Lorenzo, R. Androsch, *Eur. Polym. J.* **2015**, *70*, 215.
- [20] J. P. Kalish, K. Aou, X. Yang, S. L. Hsu, *Polymer* **2011**, *52*, 814.
- [21] C. Fosse, A. Bourdet, E. Ernault, A. Esposito, N. Delpouve, L. Delbreilh, S. Thiyagarajan, R. J. I. Knoop, E. Dargent, *Thermochim. Acta* **2019**, *677*, 67.
- [22] S. Saeidlou, M. A. Huneault, H. Li, C. B. Park, *Progr. Polym. Sci.* **2012**, *37*, 1657.
- [23] D. Garlotta, *J. Polym. Env.* **2001**, *9*, 63.
- [24] B. Wunderlich, *Thermochim. Acta* **1997**, *300*, 43.
- [25] J. Menczel, B. Wunderlich, *J. Polym. Sci., Polym. Phys.* **1980**, *18*, 1433.
- [26] B. Wunderlich, *Progr. Polym. Sci.* **2003**, *28*, 383.
- [27] M. Arnoult, E. Dargent, J. F. Mano, *Polymer* **2007**, *48*, 1012.
- [28] A. Magoń, M. Pyda, *Polymer* **2009**, *50*, 3967.
- [29] M. C. Righetti, E. Tombari, *Thermochim. Acta* **2011**, *522*, 118.
- [30] M. C. Righetti, D. Prevosto, E. Tombari, *Macromol. Chem. Phys.* **2016**, *217*, 2013.
- [31] C. Schick, R. Androsch, *Macromolecules* **2020**, *53*, 8751.
- [32] R. Androsch, A. Toda, Y. Furushima, C. Schick, *Macromol. Chem. Phys.* **2021**, *222*, 2100177.
- [33] R. Androsch, C. Schick, M. L. Di Lorenzo, *Macromol. Chem. Phys.* **2014**, *215*, 1134.
- [34] R. Androsch, E. Zhuravlev, C. Schick, *Polymer* **2014**, *55*, 4932.
- [35] Corbion personal information (10/08/2018).
- [36] Product information, www.total-corbion.com/downloads (assessed: 15/03/2022).
- [37] C. Sungkapreecha, M. J. Beily, J. Kressler, W. W. Focke, R. Androsch, *Thermochim. Acta* **2018**, *660*, 77.
- [38] J. E. K. Schawe, *Thermochim. Acta* **2015**, *603*, 128.
- [39] C. Schick, A. Toda, R. Androsch, *Macromolecules* **2021**, *54*, 3366.
- [40] A. Wurm, A. Herrmann, M. Cornelius, E. Zhuravlev, D. Pospiech, R. Nicula, C. Schick, *Macromol. Mater. Eng.* **2015**, *300*, 637.
- [41] K. Jariyavidyanont, A. Abdelaziz, R. Androsch, C. Schick, *Thermochim. Acta* **2019**, *674*, 95.
- [42] M. Schulz, A. Seidlitz, R. Kurz, R. Bärenwald, A. Petzold, K. Saalwächter, T. Thurn-Albrecht, *Macromolecules* **2018**, *51*, 8377.
- [43] A. Seidlitz, T. Thurn-Albrecht, in *Polymer Morphology* (Ed: Q. Guo), Wiley, Hoboken, NJ, USA **2016**, pp. 151–164.
- [44] R. Androsch, M. L. Di Lorenzo, *Polymer* **2013**, *54*, 6882.
- [45] R. Androsch, C. Schick, M. L. Di Lorenzo, *Adv. Polym. Sci.* **2017**, *279*, 235.
- [46] R. A. Andrianov, R. Androsch, R. Zhang, T. A. Mukhametzyanov, A. S. Abyzov, J. W. P. Schmelzer, C. Schick, *Polymer* **2020**, *196*, 122453.
- [47] S. Quattrosoldi, N. Lotti, M. Soccio, C. Schick, R. Androsch, *Polymers* **2020**, *12*, 1099.
- [48] J. D. Ferry, *Viscoelastic Properties of Polymers*, Wiley, New York, **1980**.
- [49] E. W. Fischer, G. F. Schmidt, *Angew. Chem. Int. Ed. in Engl.* **1962**, *1*, 488.
- [50] M. J. McCready, J. M. Schultz, J. S. Lin, R. W. Hendricks, *J. Polym. Sci., Polym. Phys.* **1979**, *17*, 725.
- [51] J. E. K. Schawe, S. Pogatscher, in: *Fast scanning calorimetry* (Eds: C. Schick, V. Mathot) Springer, Cham, **2016**, pp. 3–80.
- [52] M. Pyda, A. Czerniecka-Kubicka, *Adv. Polym. Sci.* **2017**, *279*, 153.
- [53] K. Aou, S. L. Hsu, L. W. Kleiner, F.-W. Tang, *J. Phys. Chem. B* **2007**, *111*, 12322.
- [54] X. Cao, A. Mohamed, S. H. Gordon, J. L. Willett, D. J. Sessa, *Thermochim. Acta* **2003**, *406*, 115.
- [55] E. Lizundia, S. Petisco, J.-R. Sarasua, *J. Mech. Beh. Biomed. Mater.* **2013**, *17*, 242.
- [56] X. Monnier, N. Delpouve, N. Basson, A. Guinault, S. Domenek, A. Saiter, P. E. Mallon, E. Dargent, *Polymer* **2015**, *73*, 68.
- [57] X. Monnier, A. Saiter, E. Dargent, *Thermochim. Acta* **2017**, *648*, 13.
- [58] L. Aliotta, M. Gazzano, A. Lazzeri, M. C. Righetti, *ACS Omega* **2020**, *5*, 20890.
- [59] U. W. Gedde, *Essential classical thermodynamics* Springer, Cham, **2020**.
- [60] C. Schick, A. Wurm, A. Mohamed, *Colloid Polym. Sci.* **2001**, *279*, 800–800.
- [61] C. Schick, A. Wurm, A. Mohammed, *Thermochim. Acta* **2003**, *396*, 119.
- [62] A. Wurm, M. Ismail, B. Kretzschmar, D. Pospiech, C. Schick, *Macromolecules* **2010**, *43*, 1480.
- [63] J. Lin, S. Shenogin, S. Nazarenko, *Polymer* **2002**, *43*, 4733.
- [64] R. H. Boyd, *Polymer* **1985**, *26*, 1123.
- [65] W. Chen, W. Zhou, Y. Makita, S. Wang, S. Yuan, T. Konishi, T. Miyoshi, *Macromol. Chem. Phys.* **2018**, *219*, 1700451.
- [66] X. Ling, J. E. Spruiell, *J. Polym. Sci., Polym. Phys.* **2006**, *44*, 3378.
- [67] X. Ling, J. E. Spruiell, *J. Polym. Sci., Polym. Phys.* **2006**, *44*, 3200.
- [68] S. Baratian, E. S. Hall, J. S. Lin, R. Xu, J. Runt, *Macromolecules* **2001**, *34*, 4857.
- [69] B. Wunderlich, *Macromolecular Physics, Vol. 3*, Academic Press, New York **1980**.
- [70] Y. Tanabe, G. R. Strobl, E. W. Fischer, *Polymer* **1986**, *27*, 1147.
- [71] T. Albrecht, G. Strobl, *Macromolecules* **1995**, *28*, 5827.
- [72] W. Hu, T. Albrecht, G. Strobl, *Macromolecules* **1999**, *32*, 7548.
- [73] B. Goderis, H. Reynaers, R. Scherrenberg, V. B. F. Mathot, M. H. J. Koch, *Macromolecules* **2001**, *34*, 1779.
- [74] A. Toda, Y. Furushima, R. Androsch, C. Schick, *Polymer* **2021**, *230*, 124057.
- [75] The increase of the melting temperature depends on its absolute value. For melting temperatures of 445, 453, and 463 K, the increases are 2.3, 1.2, and 0.5 K nm⁻¹, respectively. These melting temperatures correspond to lamellar thicknesses of 15, 20, 31 nm. All estimates are based on values of T_{m,0}, Δh_{m,100}, and σ_e [= fold surface free energy] reported in ref. [75].
- [76] R. Vasanthakumari, A. J. Pennings, *Polymer* **1983**, *24*, 175.
- [77] W. Hoogsteen, A. R. Postema, A. J. Pennings, G. Ten Brinke, P. Zugenmaier, *Macromolecules* **1990**, *23*, 634.
- [78] J. Kobayashi, T. Asahi, M. Ichiki, A. Oikawa, H. Suzuki, T. Watanabe, E. Fukada, Y. Shikinami, *J. Appl. Phys.* **1995**, *77*, 2957.
- [79] K. Wasanasuk, K. Tashiro, M. Hanesaka, T. Ohhara, K. Kurihara, R. Kuroki, T. Tamada, T. Ozeki, T. Kanamoto, *Macromolecules* **2011**, *44*, 6441.
- [80] I. M. Hodge, *Macromolecules* **1983**, *16*, 898.
- [81] P. Pan, B. o Zhu, Y. Inoue, *Macromolecules* **2007**, *40*, 9664.